Materials Science and Engineering C 28 (2008) 1408–1413

Contents lists available at ScienceDirect

Materials Science and Engineering C

journal homepage: www.elsevier.com/locate/msec

Evaluation on corrosion behavior and haemocompatibility of phosphorus incorporated tetrahedral amorphous carbon films

Aiping Liu *, Jiecai Han, Jiaqi Zhu, Songhe Meng, Xiaodong He

Center for Composite Materials, Harbin Institute of Technology, P.O. Box 3010, Yikuang Street 2, Harbin 150080, China

ARTICLE INFO

Article history:
Received 18 September 2007
Received in revised form 2 March 2008
Accepted 18 March 2008
Available online 27 March 2008

PACS:
81.05.Uw
82.45.Bb
87.68.+z
81.15.Ef
81.05.Bx

Keywords:
Filtered cathodic vacuum arc
Electrochemical corrosion
Haemocompatibility
Phosphorus incorporated tetrahedral amorphous carbon (ta-C:P)

ABSTRACT

Phosphorus incorporated tetrahedral amorphous carbon (ta-C:P) films are deposited on biomedical titanium alloy (Ti6Al4V) by filtered cathodic vacuum arc technique. The structural properties of ta-C:P films are evaluated by X-ray photoelectron spectroscopy and Raman spectroscopy. Potentiodynamic polarization tests are employed to assess the corrosion performances of ta-C:P coated and uncoated Ti alloys in 0.89 wt.% NaCl solution. In vitro platelet adhesion measurements are performed to investigate the blood compatibility of ta-C:P films. Results indicate that phosphorus incorporation increases the corrosion resistance of ta-C films. More positive breakdown potential and lower corrosion current density than those of Ti alloy are observed for ta-C:P films. Lower platelet adhesion and activation demonstrate the enhanced haemocompatibility of Ti alloy coated with ta-C:P films. The improved interaction between ta-C:P films and biological environments is attributed to structural changes of the films after phosphorus introduction.

1. Introduction

Amorphous carbon (a-C) and tetrahedral amorphous carbon (ta-C) have attracted considerable attention as biomedical implant coatings [1–7] and bioelectronic devices [8–10], such as biosensors for in vivo detection, due to their excellent mechanical properties, low coefficient of friction, good biocompatibility, high wear resistant, long-term stability and chemical inertness against aggressive media including blood. However, the film with rich-sp^3 fraction has high intrinsic compressive stress, which severely harms film adhesion to biomedical substrates and limits film practical application [11]. Moreover, the film prepared by physical or chemical phase deposition technology is usually porous [12]. These pores become the channels of chemical solution permeating into the film and dissolving the substrate. To obtain biocompatible a-C film with high corrosion resistant and good adhesion, many techniques were developed during the film deposition. Plasma-surface modification, such as plasma immersion ion implantation technique was an effective approach to meliorate surface and interface characteristics of materials [13]. With amorphous silicon or SiC as an intermediate layer, graded a-C films showed good adhesion on metal implants [11,14–16]. Furthermore, impurity doping was one of the promising methods to enhance adhesion strength and corrosion resistance of films. Many efforts were devoted to the introduction of additional elements, such as fluorine, nitrogen, silicon and metals into carbonaceous structures to improve the biological compatibility [17–22] and anticorrosive ability of films [23–27].

As a composition of life, phosphorus was incorporated into diamond-like carbon film and the resulted material was compatible with blood [28]. Previous studies also reported the application of conductive phosphorus doped a-C (a-C:P) film in semiconductor devices [29–31] and showed the potential capability of phosphorus incorporated tetrahedral amorphous carbon (ta-C:P) film as an electrochemical electrode [32]. Considering the acceptability of ta-C:P film for in vivo detection, corrosive resistance and blood compatibility should be designedly evaluated. However, not much attention is paid to the investigation of corrosion behavior when phosphorus is incorporated into carbon films, although the property is of very importance for the use of materials in either chemical or biological environment.

In the present work, ta-C:P films are synthesized on biomedical titanium alloys by filtered cathodic vacuum arc (FCVA) technique. FCVA is one of the favorable methods to prepare ta-C films with excellent mechanical properties and biocompatibility [33,34]. PH_3 widely used in the semiconductor industry is adopted as the dopant

* Corresponding author. Tel.: +86 451 86402954; fax: +86 451 86417970.
E-mail address: liuaiping1979@gmail.com (A. Liu).

0928-4931/$ – see front matter © 2008 Elsevier B.V. All rights reserved.
doi:10.1016/j.msec.2008.03.007

Table 1
Deposition parameters of ta-C and ta-C:P films with different phosphorus contents obtained from XPS analyses

Material	PH_3 flow rate (sccm)	PH_3 partial pressure (Torr)	Cathode current (A)	Substrate bias (V)	P/(P+C) (at.%)
ta-C	0	0	60	−80	0.0
ta-C:P-1	2	8.2×10^{-6}	60	−80	2.9
ta-C:P-2	8	6.4×10^{-5}	60	−80	5.8
ta-C:P-3	15	1.2×10^{-4}	60	−80	8.1

The relative error of all data is less than 5%.

source. X-ray photoemission spectroscopy (XPS) and Raman spectroscopy are performed to assess the components and microstructures of ta-C:P films. The corrosion performances of ta-C:P films are examined by potentiodynamic polarization measurements in 0.89 wt.% NaCl solution. The surface morphologies of the films after corrosion tests are discussed via scanning electron microscopy (SEM). The platelet behaviors including adhesion, spreading and morphology are assessed by in vitro platelet adhesion and activation experiments, SEM and computerized image analysis. This study may be helpful in guiding the selection of materials for the application in blood-contacting devices.

2. Experimental details

2.1. Film preparation

Biomedical titanium alloy (Ti6Al4V) was used as the substrate and reference material. Ti alloy specimens were cut into cylinders, 10 mm in diameter and 2 mm in thickness. Then the specimens were ground and polished to obtain a mirror-like surface, and cleaned with acetone, ethanol and distilled water in an ultrasonic cleaner.

ta-C and ta-C:P films with the thickness about 200 nm were deposited on silicon and Ti alloy substrates by FCVA system described elsewhere [32]. Before deposition, the substrates were placed in the plasma working chamber and etched with argon plasma for 10 min to eliminate the natural oxide layer. Three ta-C:P films were prepared by controlling the flow rate of PH_3 gas (purity 99.9999%) during the deposition. Details of experimental parameters were displayed in Table 1.

2.2. Film characterizations

XPS analysis was made using a PHI ESCA 5700 spectrometer with Al K_α (1486.6 eV) as the X-ray source. XPS core level spectra of C 1s and P 2p were scanned at 0.125 eV step with a pass energy of 30 eV. Surface chemical compositions of the films were analyzed and quantified for phosphorus and carbon elements from the peak areas corresponding to P 2p and C 1s spectra and the sensitivity factors of instrument:

$$\%X = \left(\frac{A_X}{S_X}\right) / \sum_{i=1}^{N}\left(\frac{A_X}{S_X}\right)$$

where X is the element; A_X is the area of peak for element X; S_X is the sensitivity factor for element X. Raman analysis over the range from 800 to 2000 cm^{-1} was performed at room temperature on a Jobin Yvon Labram HR 800 spectrometer with 458-nm Ar^+ laser as the excitation source.

Potentiodynamic polarization experiments were carried out on a computer-controlled potentiostat (PARSTAT 2273, USA) in 0.89 wt.% NaCl solution (pH 7.4) at 37 °C. A conventional three-electrode system consisted of saturated calomel electrode (SCE) as reference electrode and platinum as counter electrode. The uncoated and coated Ti alloys were employed as the testing specimens with their edges and backsides sealed by O-ring resins. Potentiodynamic polarization curves were measured at a rate of 1 mV/s after the specimens were immersed in the experimental solution for 6 h under open circuit conditions. Surface morphologies of all specimens after corrosion tests were examined by SEM (HITACHI S-4700, Japan).

In vitro platelet adhesion experiments were conducted using human whole blood taken from a healthy donor. After centrifugation, red cells and platelets were separated and platelet-rich plasma (PRP) was obtained. Three identical samples of per material were cleaned and incubated in PRP for 60 min at 37 °C. After rinsing, fixing, and critical point drying, all samples were studied using SEM.

Two parameters were chosen to evaluate spreading and morphology of platelets on the materials. The degree of platelet spreading on material surfaces was assessed by the index of platelet size (S) which was defined as the ratio of area coverage of platelets (A_p) in a randomly sampled area to the number of individual platelets (N) in the same area: $S=A_p/N$. Platelet morphology was evaluated by circularity index (C) proposed by Park [35]: $C=P^2/4\pi A$, where P and A were the perimeter and area of platelets, respectively. For obtaining these two parameters, image analysis software was used to distinguish the labeled platelet cytoskeletons from the background and measure their areas and perimeters.

2.3. Statistical analysis

Platelet adhesion on ten fields (1.21×10^{-2} mm^2 per field at a magnification factor of 1000) for per sample of per material was quantified and the average counts from the thirty fields were evaluated by stereological analysis [36] and computer-aided image analysis software. Comparison of the results between different materials used the analysis of variance (ANOVA) with a statistical difference of $p<0.05$ or $p<0.01$.

The area and perimeter of adhered platelets were measured on three parallel samples per material. The averages of platelet areas and circularity indexes were compared between different materials using ANOVA ($p<0.05$ or $p<0.01$).

3. Results and discussion

3.1. Microstructures of ta-C:P films

Fig. 1 shows a typical XPS overview of ta-C and ta-C:P-2 films. The peak centered at 285.5±0.2 eV is caused by the photoelectrons excited from C 1s spectra. A slight shift of C 1s spectrum towards a lower binding energy is detected by the addition of phosphorus. The two peaks located at 132.4±0.2 eV and 189.5±0.2 eV are attributed to P 2p and P 2s spectra, respectively. An oxygen signal at 533.2±0.2 eV is the result of air exposure during the experiment and sample transport. The content of phosphorus over the sum of phosphorus and carbon

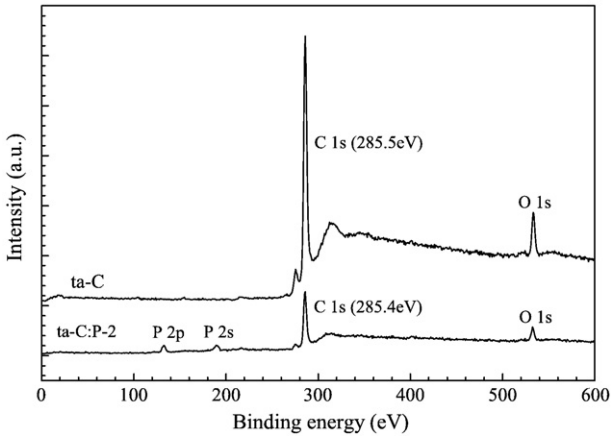

Fig. 1. XPS spectra of ta-C and ta-C:P films with 8-sccm PH_3 introduced.

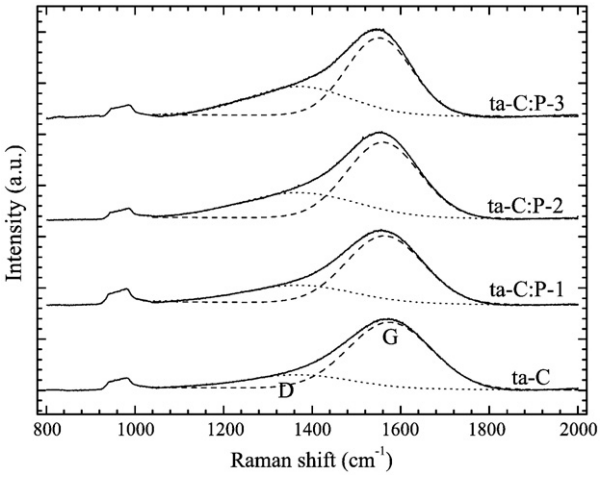

Fig. 2. Raman spectra of ta-C and ta-C:P films with different phosphorus contents. Thin solid lines are the measurements; dash lines are fitted D and G peaks.

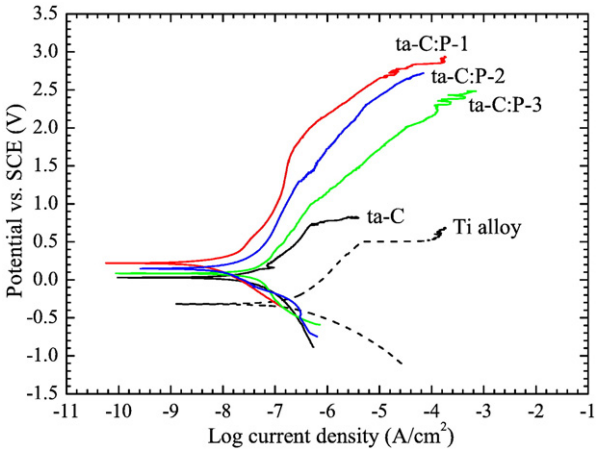

Fig. 4. Polarization curves of uncoated and ta-C and ta-C:P coated Ti alloys in 0.89 wt.% NaCl solution.

(P/(C+P)) is observed to increase from 0 to 8.1 at.% as the flow rate of PH_3 increases from 0 to 15 sccm (Table 1).

Raman spectra of ta-C and ta-C:P films shown in Fig. 2 illustrate that the lineshapes of all spectra are similar and demonstrate the amorphous structures of the films. The peak centered at about 980±2 cm^{-1} is the second-order peak of silicon. We fit the asymmetric first-order band of carbon between 1000 and 1800 cm^{-1} with D peak centered at about 1370±5 cm^{-1} and G peak centered at 1560±15 cm^{-1}. When PH_3 flow rate varies from 0 to 15 sccm, the intensity ratio of D and G peaks, I_D/I_G, exhibits a slight increase from 0.20 to 0.37, accompanied with a pronounced fall in the full width at half maximum (FWHM) of G peak from 219.2 to 173.1 cm^{-1} (Fig. 3). The increase of I_D/I_G ratio indicates an increased content of sp^2-hybridized carbon atoms in the film and the clustering of sp^2 groups, especially, an evolution of sp^2 configurations from olefinic groups to rings [37]. This result is practically identical to the downshift of G peak from 1574.8 to 1551.0 cm^{-1} because aromatic bonds are longer than olefinic bonds in chains and hold lower vibration frequencies [37]. The lower FWHM of G peak at higher phosphorus content may result from the removal of strain in bond angle and bond length due to the stress relief of ta-C:P films [38].

3.2. Electrochemical corrosion behavior

Fig. 4 shows the potentiodynamic polarization curves of Ti alloys uncoated and coated with ta-C and ta-C:P films in 0.89 wt.% NaCl solution. The corrosion potential (E_{corr}), breakdown potential (E_{brk}) and corrosion current density (I_{corr}) of all materials obtained from the curves are summarized in Table 2. It can be seen that E_{corr} and E_{brk} of ta-C film are higher and I_{corr} is one order of magnitude lower than those of Ti substrate. More obvious changes in E_{corr}, E_{brk} and I_{corr} can be observed for ta-C:P films. The whole polarization curves of ta-C:P films move to the region of higher potential and lower current density after the incorporation of phosphorus. ta-C:P-1 film remains in passive state within a broad potential range from 223 to 1800 mV before the critical pitting potential, E_{brk} is reached. After that the anodic current density of ta-C:P-1 film increases steeply, indicating the breakdown of ta-C:P-1 passive layer. In contrast, passive regions of ta-C:P-2 and ta-C:P-3 films are narrower. ta-C:P-2 is not completely destroyed but exhibits localized breakdown at the potential about 1300 mV, and ta-C:P-3 film represents the quickest failure among the three ta-C:P films. In general, the material with lower I_{corr} and higher E_{corr} indicates better corrosion resistance. This hints that the anticorrosive performances of these specimens satisfy the rule: ta-C:P-1>ta-C:P-2>ta-C:P-3>ta-C>Ti. Ti alloy is therefore effectively protected due to the existence of passive ta-C:P films which may provide pronounced resistance to pitting and crevice corrosions in the biological solution.

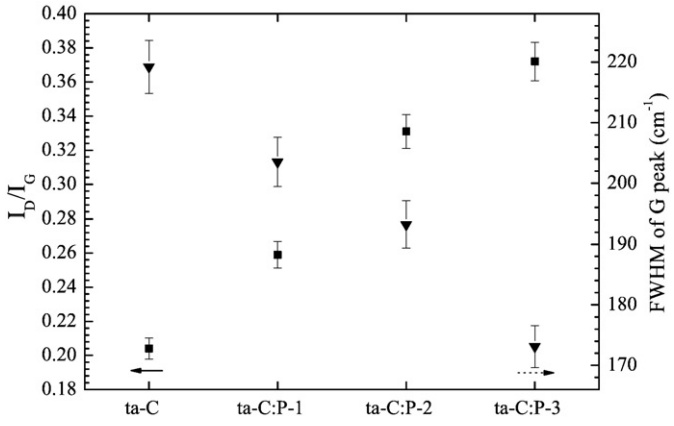

Fig. 3. I_D/I_G ratio and FWHM of G peak for ta-C and ta-C:P films.

The analysis of polarization resistance (R_P), total porosity (P_t) and protective efficiency (P_i) for ta-C and ta-C:P films (Table 2) using the method provided by Mattes [39] and Kim [15] also confirms the conclude mentioned above. The surface of Ti alloy after potentiodynamic polarization tests represents severe pitting corrosion and copious pitting holes (Fig. 5a and b). When ta-C film is coated on Ti alloy, the R_P increases and P_t decreases for ta-C/Ti specimen in terms of the contribution of high-sp^3-content, low-conductive compact ta-C film. ta-C therefore demonstrates less pitting corrosion and higher chemical inertness to Cl ions (Fig. 5c and d). However, the existent

Table 2
Results obtained from potentiodynamic polarization curves of uncoated and coated Ti alloys

Material	E_{corr} (mV)	E_{brk} (mV)	I_{corr} (A/cm^2)	R_P (MΩ cm^2)	P_t (%)	P_i (%)
Ti alloy	−326	504	2.19×10^{-7}	0.33	–	–
ta-C	31	733	4.68×10^{-8}	2.16	0.47600	78.63
ta-C:P-1	223	>1800	1.15×10^{-8}	9.73	0.00437	94.75
ta-C:P-2	150	>1300	2.24×10^{-8}	4.79	0.01177	89.77
ta-C:P-3	82	>980	3.89×10^{-8}	2.42	0.07595	82.24

The relative error of all data is less than 5%.

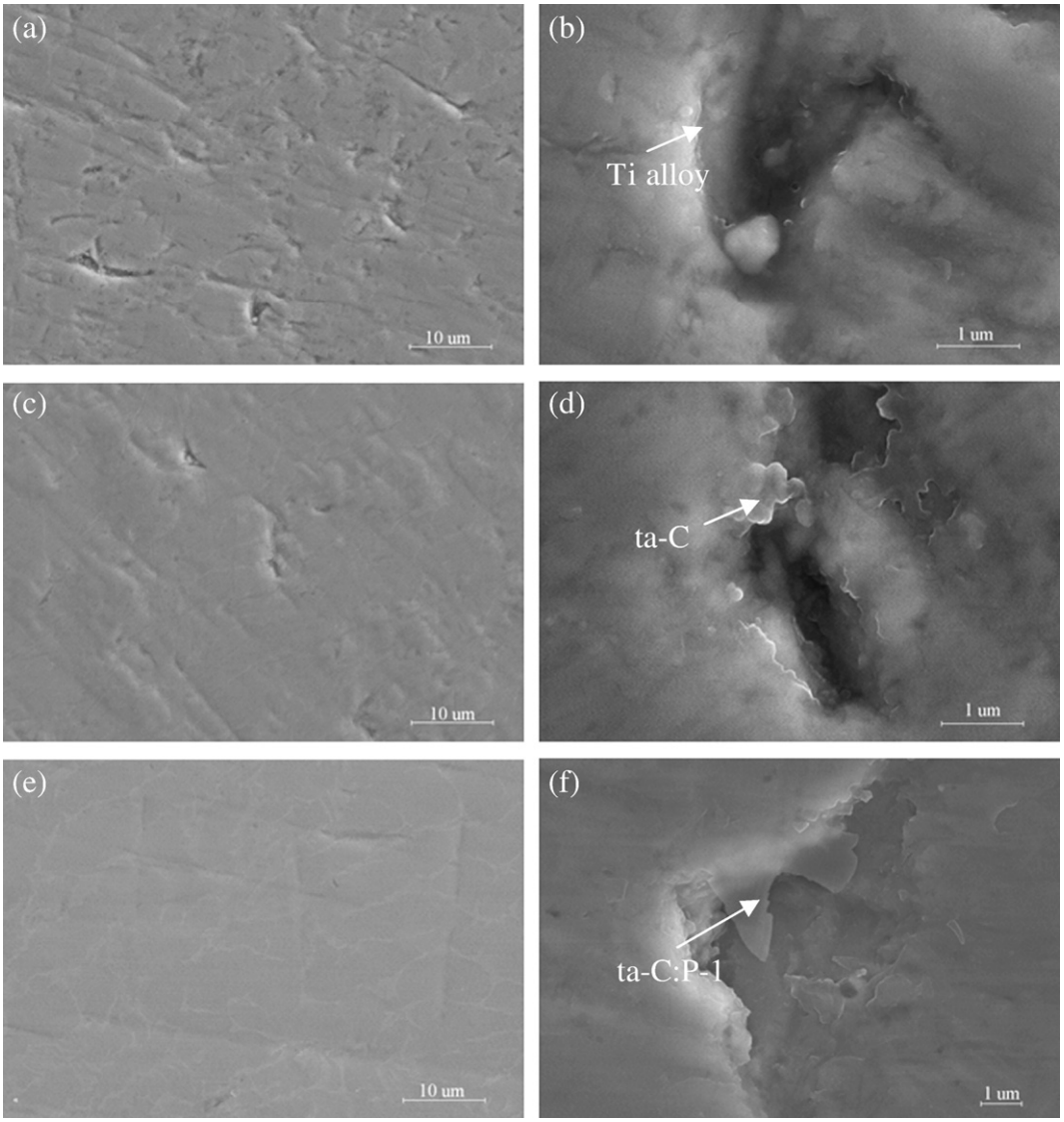

Fig. 5. SEM pitting micrographs after polarization tests: (a) and (b) for Ti alloy; (c) and (d) for ta-C film; (e) and (f) for ta-C:P-1 film.

micropores, especially, open pores in ta-C surface, will act as initial sites for the breakdown of passive layer after a long-term dipping [40]. The galvanic corrosion can be established under the difference of electrochemical potentials between the film and the substrate when Cl ions reach the interface of Ti-ta-C [16]. As a small quantity of phosphorus (<3 at.%) is incorporated in the carbon network, a slight change in the bonding structure occurs. A sharp decrease in P_t and a notable increase in R_P are observed for ta-C:P-1/Ti specimen. Furthermore, the compressive stress in ta-C:P-1 film is released [38], which might play a significant role in the improvement of adhesion strength between ta-C:P-1 and Ti substrate. Therefore, the localized defects including micropores in the interface may decrease and the penetration of solution may be restrained availably [41]. The morphology of ta-C:P-1 film after corrosion test hints its destruction through less but bigger holes compared with ta-C film (Fig. 5e and f). This can be explained by the suggestion that less pinholes and smaller anodic area of ta-C:P-1 film make the corrosive attack to the remaining pinholes heavier [29,42]. With the further increase of phosphorus fraction in ta-C film, the content of sp^2-hybridized carbon atoms remarkably increases, as discussed in Section 3.1. The graphitization of bonds destroys the compact structure and enhances the P_t of film and the probability of pitting corrosion. Therefore, low-phosphorus ta-C:P-1 film with lowest P_t and highest R_P provides the most efficient protection to Ti alloy and represents the best corrosion resistance.

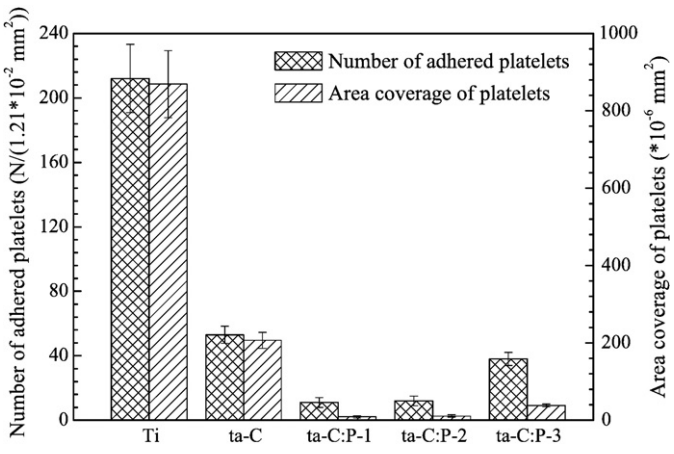

Fig. 6. Number and area coverage of adherent platelets on different surfaces.

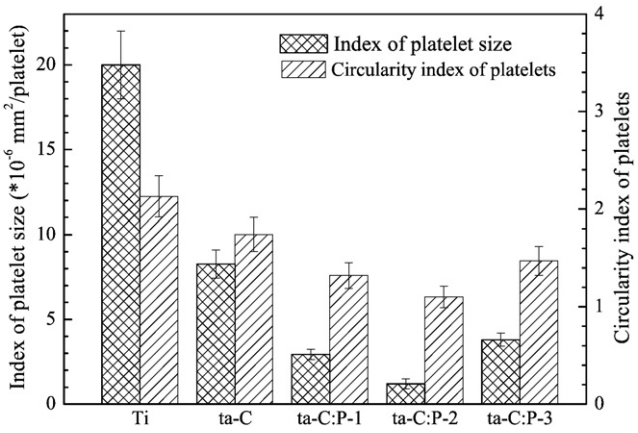

Fig. 7. Indexes of size and circularity for platelets adhered on different surfaces.

3.3. Platelet adhesion and activation

For biomedical implants contacting with blood directly, a key issue is to evaluate their ability to prevent thrombus formation. It is generally known that platelet adhesion, activation and aggregation on implant surfaces exposed to blood play an important role in the formation of a thrombus. Therefore, in vitro analysis of platelet properties is usually performed as a first assess for the haemocompatibility of a surface.

Fig. 6 plots a statistically average count and area coverage of adherent platelets in the sampled area of 1.21×10^{-2} mm^2 at 60-min incubation time. The numbers of adhered platelets on Ti alloy and ta-C surfaces are about 210 and 60 at the same area, significantly higher than those attached to ta-C:P films. A similar trend is observed from the variation of area coverage of platelets on all surfaces, namely Ti>ta-C>ta-C:P-3>ta-C:P-2>ta-C:P-1. This can be further explained from the activation degree of platelets on material surfaces. According to Goodman [43], platelet activation can be assessed by spreading degree of platelet which is related with *S*. *S* is therefore reliable in the qualitative estimation of platelet activated state. For Ti substrate, a high degree of platelet coverage combined with a low number of individual platelets (namely high *S* value as shown in Fig. 7) implies the early spread and activated state of platelets. ta-C film with a lower *S* indicates less activated action to platelets compared with Ti alloy. When <6 at.% phosphorus is introduced into ta-C film, the area coverage of platelets decreases remarkably. ta-C:P-2 with smallest *S* shows the lowest platelet spreading and activation. However, 8.1 at.% phosphorus leads to a decrease in the compatibility with blood. This

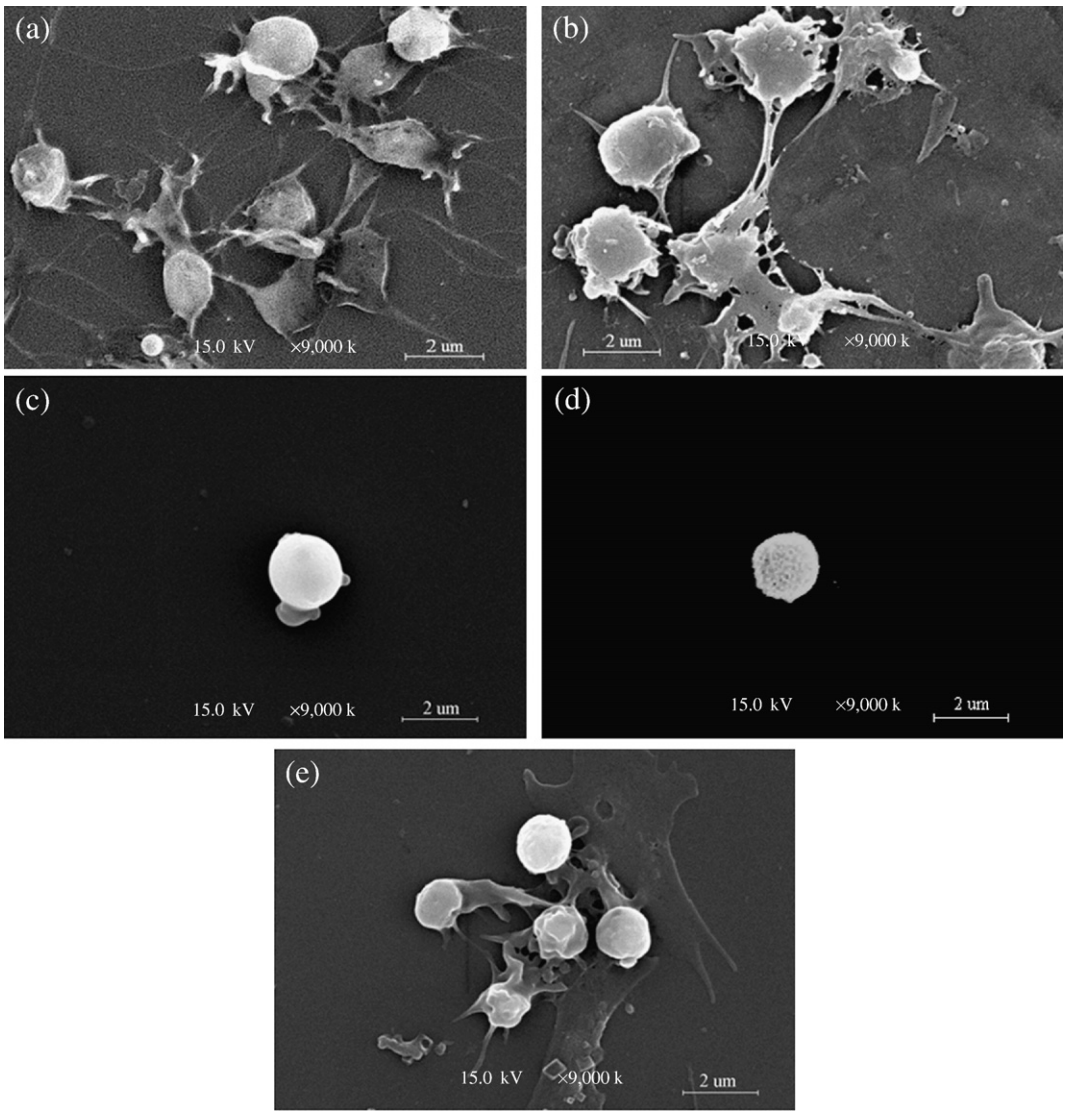

Fig. 8. Morphology of adherent platelets on (a) Ti alloy; (b) ta-C; (c) ta-C:P-1; (d) ta-C:P-2 and (e) ta-C:P-3 surface.

may be ascribed to the lower sp^3/sp^2 ratio of ta-C:P-3 film. The graphitized structure decreases the proportion of polar component in surface energy, which makes the activation of platelets on the surface stronger [5].

Additionally, morphological change of adherent platelets is a common qualitative criterion to evaluate the activation of platelets on material surfaces. Based on the model proposed by Park [35], circularity index *C* of platelet on a material is correlated with the haemocompatibility of blood-contacting surfaces. When the measured platelet is a perfect circle, *C* is equal to 1. An observed increase in *C* indicates the decreased haemocompatibility of the surface and activated state of platelets on it. As shown in Fig. 7, the high *C* of Ti hints the complex shapes of platelets on the material. The high-magnification morphology of platelets spreading on Ti alloy (Fig. 8a) confirms that the platelets with many long pseudopods appear to be mutual interactions and almost form a subconfluent layer. Although ta-C film has a lower *C*, it represents obvious activated action to the platelets which show extended pseudopods (Fig. 8b). Comparatively, most of adherent platelets on ta-C:P-1 and ta-C:P-2 films (*C* more closed to 1) remain isolated and disc shapes without pseudopod occurrence (Fig. 8c and d), indicating an unactivated or low-activated state. Not all platelets adherent to high-phosphorus ta-C:P-3 undergo shape changes at the same rate. Some platelets develop pseudopods while some are still unactivated.

In summary, successful improvement in corrosion resistance and blood compatibility of Ti alloy by ta-C:P films implies ta-C:P as a promising material for further applications in biomedical implant overcoat. It is inferred from our analyses that low contents of phosphorus can virtually meliorate the electrochemical corrosion behavior and compatibility with blood of ta-C film. However, the graphitization induced by excessive phosphorus goes against the development of anticorrosion and haemocompatibility.

4. Conclusions

In this study, the corrosion resistance and haemocompatibility of Ti alloys with and without phosphorus incorporated tetrahedral amorphous carbon (ta-C:P) films are investigated. Significant improvement in suppressing the corrosion of biological solution and effective barrier against pitting corrosion are confirmed due to the high polarization resistance and low porosity of ta-C:P films deposited on Ti alloy. Platelet spreading and morphology are numerically estimated using size and circularity indexes of platelets. Low-phosphorus ta-C:P film with lowest indexes exhibits the slightest adhesion, spreading and activation of platelets. However, high content of phosphorus increases the fraction of sp^2-hybridized carbon atoms in ta-C:P film and the ordering of structure, leading to a loss in anticorrosion and blood compatibility. Therefore, ta-C:P film with elaborately controlled phosphorus level does effectively improve the behaviors of Ti alloy in biological environment and appears to be a favorable material for biomedical implant applications.

Acknowledgments

The authors would like to thank the National Natural Science Foundation of China (Grant No. 50602012) for its financial support and Dr. Sun Mingren and Chen Yajie for their assistance provided in doing XPS and Raman measurements.

References

[1] L.A. Thomson, F.C. Law, N. Rushton, J. Franks, Biomaterials 12 (1991) 37.
[2] V.M. Tiainen, Diamond Relat. Mater. 10 (2001) 153.
[3] R. Hauert, Diamond Relat. Mater. 12 (2003) 583.
[4] A. Grill, Diamond Relat. Mater. 12 (2003) 166.
[5] P. Yang, N. Huang, Y.X. Leng, J.Y. Chen, R.K.Y. Fu, S.C.H. Kwok, Y. Leng, P.K. Chu, Biomaterials 24 (2003) 2821.
[6] R.J. Narayan, Mater. Sci. Eng., C, Biomim. Mater., Sens. Syst. 25 (2005) 405.
[7] D.H. Kim, H.E. Kim, K.R. Lee, C.N. Whang, I.S. Lee, Mat. Sci. Eng., C, Biomim. Mater., Sens. Syst. 22 (2002) 9.
[8] S.P.J. Higson, P.M. Vadgama, Anal. Chim. Acta 300 (1995) 77.
[9] R. Schnupp, R. Kuhnhold, G. Temmel, E. Burte, H. Ryssel, Biosens. Bioelectron. 13 (1998) 889.
[10] R. Maalouf, A. Soldatkin, O. Vittori, M. Sigaud, Y. Saikali, H. Chebib, A.S. Loir, F. Garrelie, C. Donnet, N.J. Renault, Mat. Sci. Eng., C, Biomim. Mater., Sens. Syst. 26 (2006) 564.
[11] N.J. Ianno, R.O. Dillon, A. Ahbad, A. Ali, Thin Solid Films 270 (1995) 275.
[12] V. Novotny, N. Staud, J. Electrochem. Soc. Electrochem. Sci. Technol. 135 (1988) 2931.
[13] P.K. Chu, J.Y. Chen, L.P. Wang, N. Huang, Mater. Sci. Eng., R Rep. 36 (2002) 143.
[14] L. Chandra, T. Clyne, M. Allen, N. Rushton, R. Butter, A.H. Lettington, Diamond Relat. Mater. 4 (1995) 852.
[15] H.G. Kim, S.H. Ahn, J.G. Kim, S.J. Park, K.R. Lee, Diamond Relat. Mater. 14 (2005) 35.
[16] C.L. Liu, D.P. Hu, J. Xu, D.Z. Yang, M. Qi, Thin Solid Films 496 (2006) 457.
[17] T. Saito, T. Hasebea, S. Yohena, Y. Matsuoka, A. Kamijo, K. Takahashi, T. Suzuki, Diamond Relat. Mater. 14 (2005) 1116.
[18] T.I.T. Okpalugo, A.A. Ogwu, P.D. Maguire, J.A.D. McLaughlin, Biomaterials 25 (2004) 239.
[19] S. Zhang, H.J. Du, S.E. Ong, K.N. Aung, H.C. Too, X.G. Miao, Thin Solid Films 515 (2006) 66.
[20] G.J. Wan, P. Yang, R.K.Y. Fu, Y.F. Mei, T. Qiu, S.C.H. Kwok, J.P.Y. Ho, N. Huang, X.L. Wu, P.K. Chu, Diamond Relat. Mater. 15 (2006) 1276.
[21] F.Z. Cui, X.L. Qing, D.J. Li, J. Zhao, Surf. Coat. Technol. 200 (2005) 1009.
[22] S.C.H. Kwok, P. Yang, J. Wang, X.Y. Liu, P.K. Chu, J. Biomed. Mater. Res. 70A (2004) 107.
[23] M.K. Fung, K.H. Lai, C.Y. Chan, I. Bello, C.S. Lee, S.T. Lee, D.S. Mao, X. Wang, Thin Solid Films 368 (2000) 198.
[24] B. Tomcik, T. Osipowicz, J.Y. Lee, Thin Solid Films 360 (2000) 173.
[25] P. Papakonstantinou, J.F. Zhao, A. Richardot, E.T. McAdams, J.A. McLaughlin, Diamond Relat. Mater. 11 (2002) 1124.
[26] D.Y. Wang, Y.Y. Chang, C.L. Chang, Y.W. Huang, Surf. Coat. Technol. 200 (2005) 2175.
[27] M.L. Morrison, R.A. Buchanan, P.K. Liaw, C.J. Berry, R.L. Brigmon, L. Riester, H. Abernathy, C. Jin, R.J. Narayan, Diamond Relat. Mater. 15 (2006) 138.
[28] S.C.H. Kwok, J. Wang, P.K. Chu, Diamond Relat. Mater. 14 (2005) 78.
[29] K.M. Krishna, M. Umeno, Y. Nukaya, T. Soga, T. Jimbo, Appl. Phys. Lett. 77 (2000) 1472.
[30] C.L. Tsai, C.F. Chen, C.L. Lin, J. Appl. Phys. 90 (2001) 4847.
[31] M. Rusop, T. Soga, T. Jimbo, Sol. Energy Mater. Sol. Cells 90 (2006) 291.
[32] A.P. Liu, J.Q. Zhu, J.C. Han, H.P. Wu, W. Gao, Electroanalysis 19 (2007) 1773.
[33] M. Ball, A. O'Brien, F. Dolan, G. Abbas, J.A. McLaughlin, J. Biomed. Mater. Res. 70A (2004) 380.
[34] C. Meunier, Y. Stauffer, A. Daglar, F. Chai, S. Mikhailov, H.F. Hildebrand, Surf. Coat. Technol. 200 (2006) 6346.
[35] K. Park, F.W. Mao, H. Park, Biomaterials 11 (1989) 24.
[36] E.R. Weibel, Stereological Methods, Volume 1, Academic Press, London, 1979.
[37] A.C. Ferrari, J. Robertson, Phys. Rev., B 61 (2000) 14095.
[38] A.P. Liu, J.Q. Zhu, J.C. Han, H.P. Wu, Z.C. Jia, Appl. Surf. Sci. 253 (2007) 9124.
[39] B. Matthes, E. Brozeit, J. Aromaa, H. Ronkainen, S.P. Hannula, A. Leyland, A. Matthews, Surf. Coat. Technol. 49 (1991) 489.
[40] A. Zeng, E. Liu, I.F. Annergren, S.N. Tan, S. Zhang, P. Hing, J. Gao, Diamond Relat. Mater. 11 (2002) 160.
[41] L.Y. Ostrovskaya, Vacuum 68 (2003) 219.
[42] A.D. Reisel, C. Schurer, G. Irmer, E. Muller, Surf. Coat. Technol. 830 (2004) 177.
[43] S.L. Goodman, M.D. Lelah, L.K. Lambrecht, S.L. Cooper, R.M. Albrecht, Scan. Electron. Microsc. 1 (1984) 279.